VIII International Conference on Fracture Mechanics of Concrete and Concrete Structures
FraMCoS-8
J.G.M. Van Mier, G. Ruiz, C. Andrade, R.C. Yu and X.X. Zhang (Eds)

INFLUENCE OF MINERAL ADMIXTURES ON FATIGUE BEHAVIOUR OF SELF COMPACTING CONCRETE - SCANNING ELECTRON MICROSCOPY AND MICROINDENTATION STUDY

T. Hemalatha*, J.M. Chandra Kishen† AND Ananth Ramaswamy†

*Scientist, Structural Engineering Research Centre
Chennai, India.
e-mail: hema24bala31@gmail.com

†Professor, Department of Civil Engineering
Indian Institute of Science, Bangalore, India.
e-mail: chandrak@iisc.ernet.in, web page: http://www.iisc.ernet.in

Key words: SCC, Fatigue, SEM, Microindentation

Abstract. The mineral admixtures added to concrete are beneficial because of its microfilling effect, workability enhancement, strength improvement etc. Fly ash and silica fume have high fineness, which decreases the porosity and pore size and increases the compressive strength. In this study, self compacting concrete (SCC) beams made with and without mineral admixtures have been subjected to variable amplitude fatigue loading and the response of the specimen is recorded by data acquisition system. The fatigue loading is applied in 0.5 kN increments after every 500 cycles. It is found that the addition of fly ash and silica fume slightly increase the fatigue life of SCC. The validity of Paris law for SCC is verified and Paris law coefficients m and C are determined for all the three SCC. Scanning electron microscopy (SEM) and microindentation techniques are also used to study the fracture processes in self compacting concrete. The SEM micrographs reveal that the damage has been taken place mainly through aggregates.

1 INTRODUCTION

In plain concrete, the material phases can broadly be classified as cement paste, aggregates and interfaces between aggregate and hydrated cement paste. Matrix of concrete made of mineral admixtures such as fly ash and silica fume improves the compressive strength of concrete. As the compressive strength increases, it is widely reported [4, 5] that the fatigue life of concrete decreases. Also, it is reported in literature [2] there is no relationship between compressive strength and fatigue life and the addition of silica fume increases the fatigue life. Guo et al. [1] studied the effect of fly ash and ground granulated blast furnace slag (GGBS) on fatigue life of concrete and concluded this admixtures improves the fatigue life of concrete. Hence, it is uncertain that the addition of fly ash and silica fume increase or decrease the fatigue life. The fatigue loading causes the physical phases to undergo microscopic changes such as opening and growth of bond cracks that exist at the interfaces between coarse aggregate and hydrated cement paste even prior to the application of load. It also causes reversed movement of aggregates along the interface, aggregate surface abrasion and damage of the interface under repeated load [9]. These microscopic changes in turn cause detrimental changes in macroscopic

material properties. Typically, the aggregate bridging force decreases with number of cycles because of the interfacial damage or aggregate breakage [10]. Hence, it can be said that fatigue damage caused to soft aggregates as well as to aggregate/matrix interfaces which is the weakest phase in concrete results in the fatigue crack growth in concrete. It is widely accepted that the mechanical properties (strength, ductility, fracture behavior etc.) at macro level are affected by the properties at the nano level [3]. In this work, the behavior of normal, medium and high strength SCC made with and without fly ash and silica fume under fatigue loading is studied. Also, the fracture processes in three SCCs have been studied using SEM and microindentation.

2 Experimental Details

2.1 Materials

Ordinary Portland Cement (OPC) conforming to Indian Standards [6] is used for this work. Natural sand (0-3mm) and gravel (3-12.5mm) are used for SCC mixtures. A "class F" fly ash that complies with the requirements of ASTM C 618 [8] and micro silica 920-D grade (ELKEM) that conforms to ASTM C 1240 [7] are used for this study. A polycarboxylate based super plasticizer incorporating viscosity modifying agent is used for enhancing the workability.

2.2 Specimen preparation and curing

The dimensions of 50 mm thick geometrically similar three point bend beams, used for fatigue testing are shown in Table 1.

Table 1: Details of geometrically similar beam dimensions for fatigue loading

Beam Designation	Depth d (mm)	Length L (mm)	Notch Size a_0 (mm)
Small	76	241	15.2
Medium	152	431	30.4
Large	304	810	60.8

The three SCC mixes are poured into their respective moulds after testing for fresh properties. The SCC prisms are demoulded after 24 hours and are cured under water for 28 days.

2.3 Testing of specimens

All the beams are simply supported and tested under three point bending configuration. A variable amplitude fatigue loading of 1 Hz frequency is applied in increments of 0.5 kN after every 500 cycles as shown in Figure 1 with the minimum load maintained at 0.2 kN.

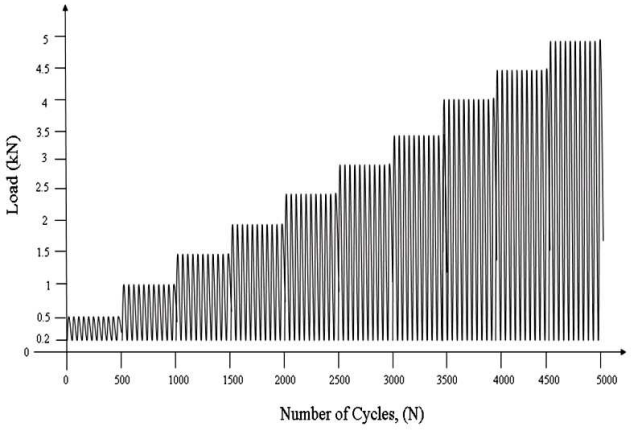

Figure 1: The typical pattern of variable amplitude loading applied in this study

The test set up includes a closed loop servo hydraulic machine of 500 kN capacity having a specially calibrated 50 kN load cell, linear variable displacement transformer (LVDT) and a clip gauge. A computer aided data acquisition system is used to monitor load and displacement throughout the testing period.

2.4 Stiffness degradation of SCC

Fracture in SCC is caused by mechanical interaction between the coarse aggregates and the cement-based matrix. The beams made of three SCC mixes are subjected to variable amplitude fatigue loading, to understand the influence of fly ash and silica fume on the fatigue behavior. The load and its resultant crack mouth opening displacement (CMOD) during the fatigue tests are continuously recorded by the data acquisition system.

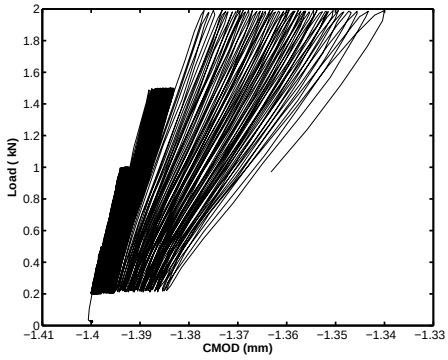

Figure 2: Typical load Vs CMOD pattern for small size specimen, under varying amplitude loading

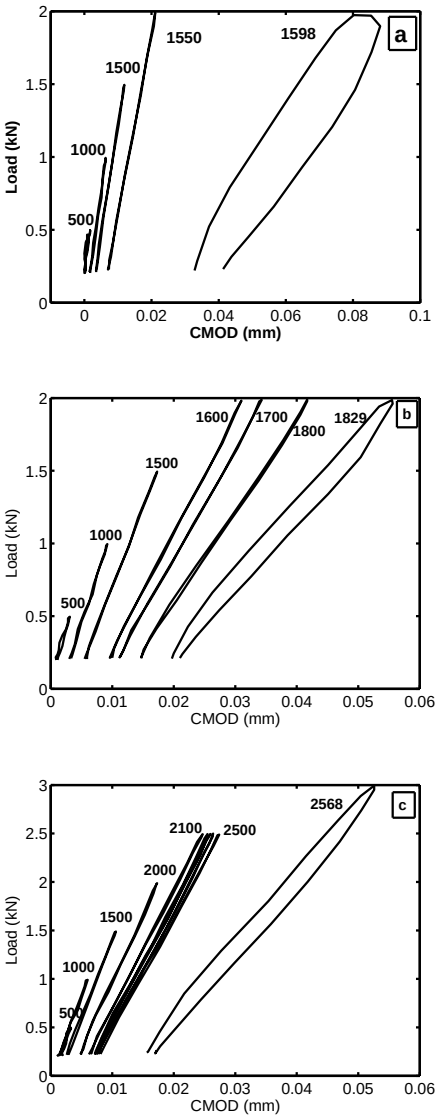

Figure 3: Load versus CMOD plot (selected cycles) of small specimens of a) SCC1 b) SCC2 and c) SCC3

A typical plot of CMOD versus number of cycles for the small sized specimen is shown in Figure 2. In this plot it is seen that the slope of the load-CMOD curve is continuously decreasing indicating the degradation in stiffness due to damage accumulation. In order to compute the decrease in stiffness, the load versus CMOD plot at every five hundredth cycle (when the amplitude changes) is plotted for small specimen as shown in Figure 3 for all the three SCC mixes. The change in flexural stiffness (secant stiffness computed between minimum and maximum load levels) during variable amplitude fatigue loading of all the three sizes of SCC1, SCC2 and SCC3 are measured. Figure 4 shows the variation of stiffness with increasing number of cycles for small sized beam and for all the three SCC mixes.

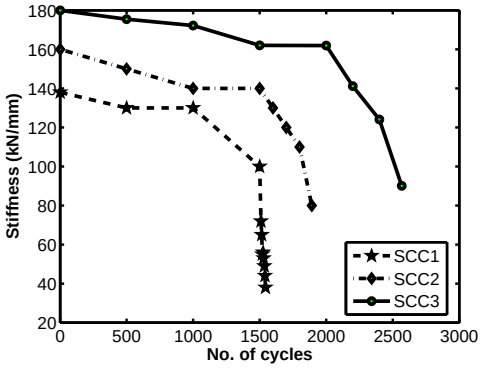

Figure 4: Stiffness of the small size beam versus number of cycles

From this plot it is seen that there is no significant change in the stiffness during initial period indicating that the rate of damage in the concrete is slow. But with increasing number of cycles, the stiffness drops considerably due to accumulation of damage that has occurred in the form of microcracks. These microcracks coalesce and forms a major crack leading to failure. Though the stiffness degradation trend is similar for all the three mixes, the initial stiffness of the three mixes are different. The initial stiffness is larger for SCC3 followed by SCC2 and SCC1. This is due to the more homogenized microstructure of SCC3 when compared

with SCC1, due to the presence of higher powder content. Further, the presence of unhydrated cement in SCC2 and SCC3 caused by the addition of class F fly ash is also responsible for the high initial stiffness of SCC2 and SCC3. Figure 5 shows the decrease in stiffness with increasing number of fatigue loading cycles for SCC3 for all the three sizes. It is seen that the behavior in terms of stiffness degradation is very similar for all the three sizes.

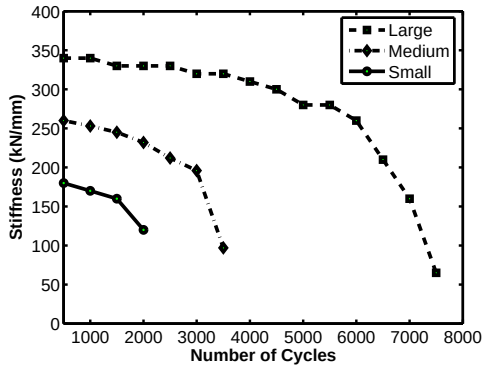

Figure 5: Stiffness of large, medium and small size specimens of SCC3

For each mix test has been conducted on three specimens each for three sizes. Hence a total of 27 specimens have been tested for fatigue. The average number of failure cycles of the three specimens for all the three mixes is presented in Table 2.

Table 2: Average number of cycles at failure of three specimens at each size for three SCC mixes (standard deviation shown within paranthesis)

Beam size	SCC1	SCC2	SCC3
	No. of cycles to failure		
Small	1509(21.6)	2085(23.3)	2535(30.8)
Medium	3085(16.3)	3290(31.1)	3505(1.50)
Large	6003(6.50)	6538 (45.6)	7072(32.9)

For a particular concrete, the failure number of cycles increases with increase in size. This is on similar lines as observed in the average peak loads under monotonic loading for different sizes as listed in Table 3.

Table 3: Average peak loads of beams from monotonic test

Beam size	SCC1	SCC2	SCC3
	Average peak load (kN)		
Small	2.035	2.924	4.204
Medium	3.960	5.020	6.550
Large	6.402	8.570	11.54

For a given size of beam, the failure number of cycles increases for SCC1, SCC2 and SCC3 in that order. Once again this is expected since the corresponding average peak loads increase in the static tests in the order of SCC1, SCC2 and SCC3. The reasons for increase in failure number of load cycles for SCC3 and SCC2 when compared to SCC1 is due to improved microstructure of the concrete due to higher powder content. With higher powder content and presence of silica fume in SCC3, the porosity in the microstructure of SCC3 decreases thereby increasing its stiffness and its load carrying capacity. According to the literature [5, 11], the number of cycles to failure in high strength concrete is less when compared to normal strength concrete. Contrarily, in this study, it is found that the higher strength SCC fails at more number of cycles. This indicates that failure under fatigue loading does not depend absolutely on the compressive strength alone. Higher compressive strength could be achieved in a number of ways. It is the microstructure which actually governs the fatigue behavior of the concrete as seen in the present test results. Although the brittleness of SCC3 is the highest, due to its improved microstructure, the number of cycles to failure under fatigue is higher when compared to SCC1.

2.5 Fatigue crack growth rate

According to the fatigue theory of fracture mechanics [12], the crack growth depends on the amplitude of the stress intensity factor range (ΔK_I), for the current effective elastic crack length (a). The earliest law for describing the rate of crack growth was proposed by Paris and Erdogan [13] and is given by

$$\frac{da}{dN} = C\,(\Delta K)^m \tag{1}$$

where da/dN is the crack growth per cycle, ΔK is the stress intensity range, C and m are material constants. In log-log grid, da/dN and ΔK is expressed as a straight line with an intercept of $logC$ and slope m. The line segment is used for fitting the data point during stable crack propagation. According to Bazant and Xu [14], the Paris law is not applicable for concrete due to strong strength dependency on size and therefore they proposed a size adjusted Paris law [14] given by

$$\frac{da}{dN} = C\left(\frac{\Delta K}{K_{IC}}\right)^m \tag{2}$$

where K_{IC} is the mode I fracture toughness of the material. Equation (2) can be reduced to a linear regression plot by plotting log(da/dN) versus log($\Delta K/K_{IC}$).

In this work, the size adjusted Paris law given by Equation 2 is used to study the rate of crack growth and to obtain the Paris law coefficients C and m. The stress intensity factor range for a three point bend beam is computed using [11]

$$\Delta K = \frac{\Delta P f(a/D)}{b\sqrt{D}} \tag{3}$$

where $\Delta P = P_{max} - P_{min}$ is the load range, b is the beam thickness, D is the beam depth and $f(a/D)$ is a function depending on the specimen geometry. Making use of the normalized crack length curves of Figure 6 and computing ΔK using Equation 3 for a given crack size (a), a plot of log(da/dN) versus log($\Delta K/K_{IC}$) is plotted for all the three SCC mixes as shown in Figure 7.

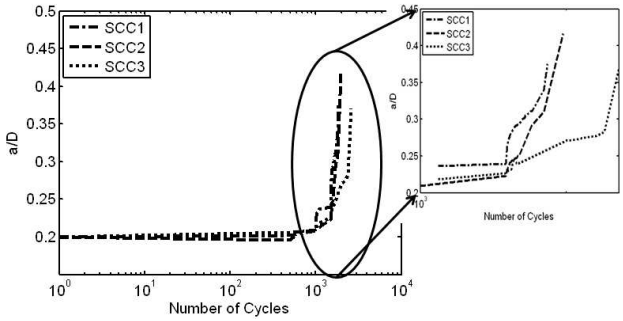

Figure 6: Relative crack length versus number of cycles for the small sized specimens

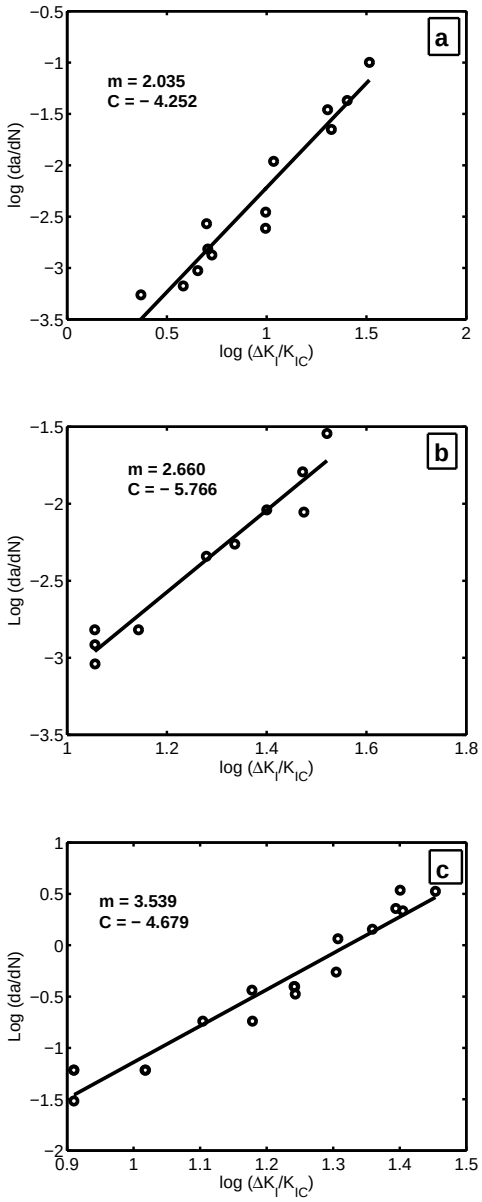

Figure 7: Fatigue crack growth rate of large specimen for a) SCC1 b) SCC2 c) SCC3

From this plot the Paris law constants m and C are computed and the results are tabulated in Table 4 for all specimen sizes.

Table 4: Paris law constants for large, medium and small size specimens of the three SCC mixes

	Mix	m	C
Large	SCC1	2.035	0.0142
	SCC2	2.660	0.0031
	SCC3	3.539	0.0093
Medium	SCC1	1.419	0.0095
	SCC2	1.516	0.0123
	SCC3	3.051	0.0015
Small	SCC1	0.600	0.0617
	SCC2	1.229	0.0332
	SCC3	1.260	0.0201

From the available literature, the constant m for ductile materials [15] falls in the range of 2.4 to 3.7 while for brittle ceramics [15] it is in the range of 24 to 131. Although, metals and ceramics have a homogeneous microstructure, their m values are significantly different. Brittle materials have a higher m value compared to the ductile materials. In this study, the Paris exponent (m) is higher for SCC3 followed by SCC2 and SCC1 as seen from Table 4. This implies that SCC3 is more brittle than SCC1 and the rate of crack growth is higher in SCC3.

2.6 Analysis of fractured surface using scanning electron microscopy

Small flaws or discontinuities are present internally or on the body surface of heterogeneous material like concrete. At these flaws, the stresses are very high due to stress concentrations effects. As a result, under cyclic loading, cracks can grow at these flaws even if the applied normal stresses are lower than the elastic limit. The SEM images taken along the fractured surface of failed specimen show various failure patterns. The pores present in the microstructures act like crack arrestor as well as crack initiator. The SCC1 which is made using less powder content has more pores. But at complete hydration, these pores are filled with hydration products. Hence, a propagating crack is arrested by these pores, preventing it from further progression as shown in Figure 8.

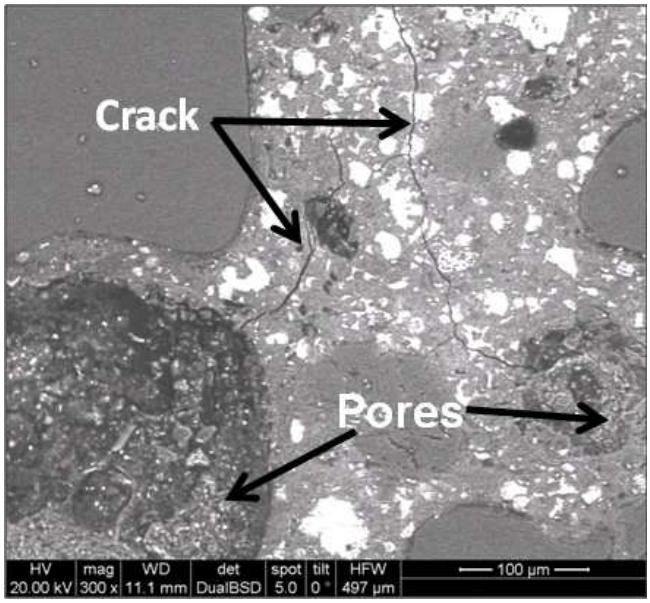

Figure 8: Crack arrest by pores in SCC1

The pores are less in number in SCC2 as well as in SCC3 due to more powder content and less water to powder ratio. The mechanism of failure observed in monotonic loading is different from that under fatigue loading. Under fatigue loading the crack is found to pass through the aggregates. Though the cracks in SCC are passing through the aggregates, the crack growth rate is slow compared to NVC. This may be due to the strong coarse aggregate used in this study.

In order to investigate the microstructural manifestation of damaging effects, images of the cross section of fractured surface are captured. Interfacial microcracks (at aggregate-paste interfaces) as well as aggregate microcracks are present in concrete. In all the three SCC mixes, it is found that the cracks pass through the aggregates causing different types of damages on and through the aggregate as shown in Figure 9.

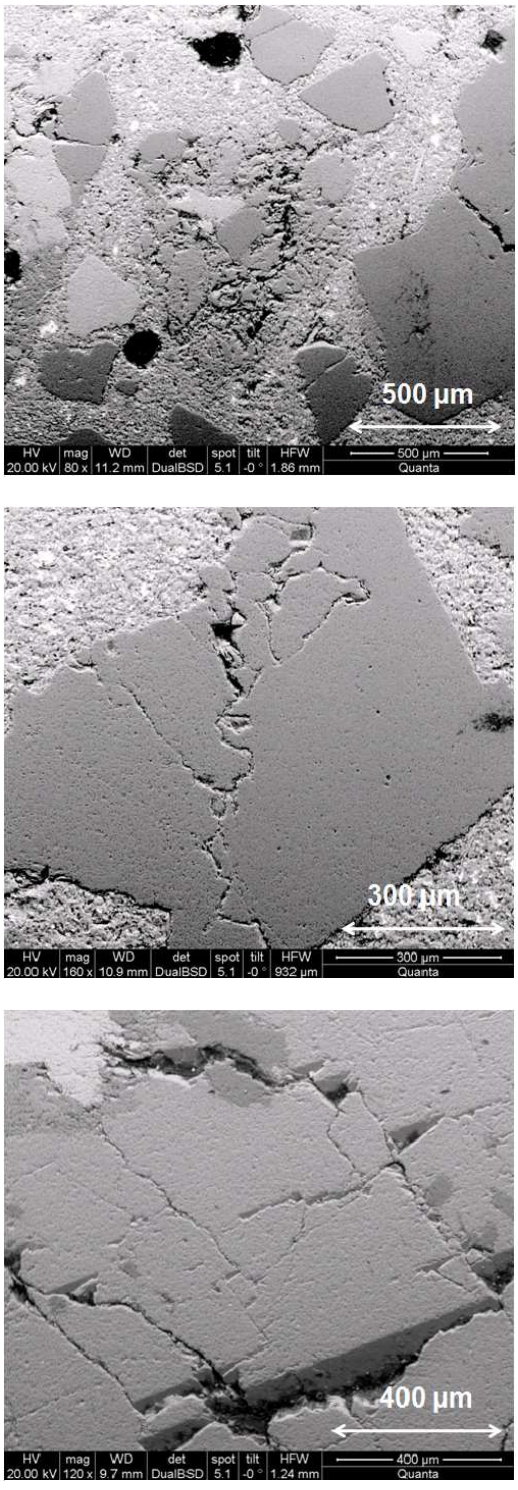

Figure 9: Damage caused on aggregates due to fatigue loading, at different magnifi cations

The typical image of crack in SCC2 and its enlarged view are shown in Figure 10. As seen in the figure, the crack passes through the aggregate. An enlarged view of the damage in SCC3 is shown in Figure 11. It is seen that there is considerable abrasion between the coarse aggregates.

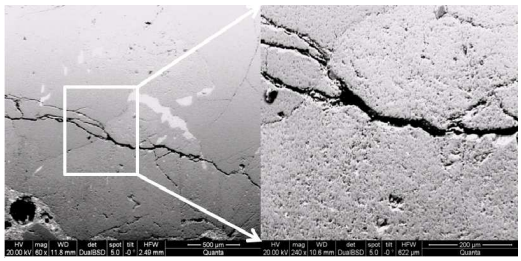

Figure 10: Crack passing through the aggregates in SCC2

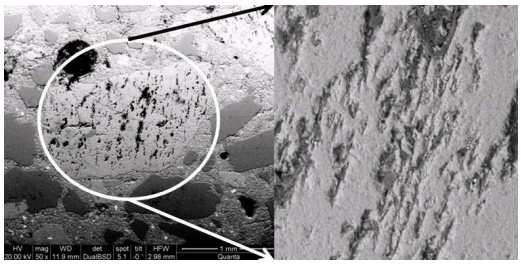

Figure 11: Abrasion on aggregate due to repeated loading on SCC3

The propagation and networking of microcracks along interfaces and into the paste is observed rarely in SCC1. Arresting and shifting of microcracks by voids and aggregates are occasionally observed in both normal-strength and high-strength SCC. Aggregate surface abrasion is noticed in all the three SCC mixes, irrespective of their strength.

2.7 Micromechanical properties of SCC under fatigue loading through microindentation

The elastic properties obtained at microlevel helps in identifying the macrolevel properties. To determine the micromechanical properties under fatigue loading, several indentation tests are performed at different points of the concrete samples of all the three SCC mixes. Samples of the three mixes are subjected to a constant multicycle load with a minimum load amplitude of 0.2 N and a maximum load of 5.0 N. Each indented point has a different depth of penetration which provides an idea about the properties of

that material. The softer the material, higher is the depth of penetration.

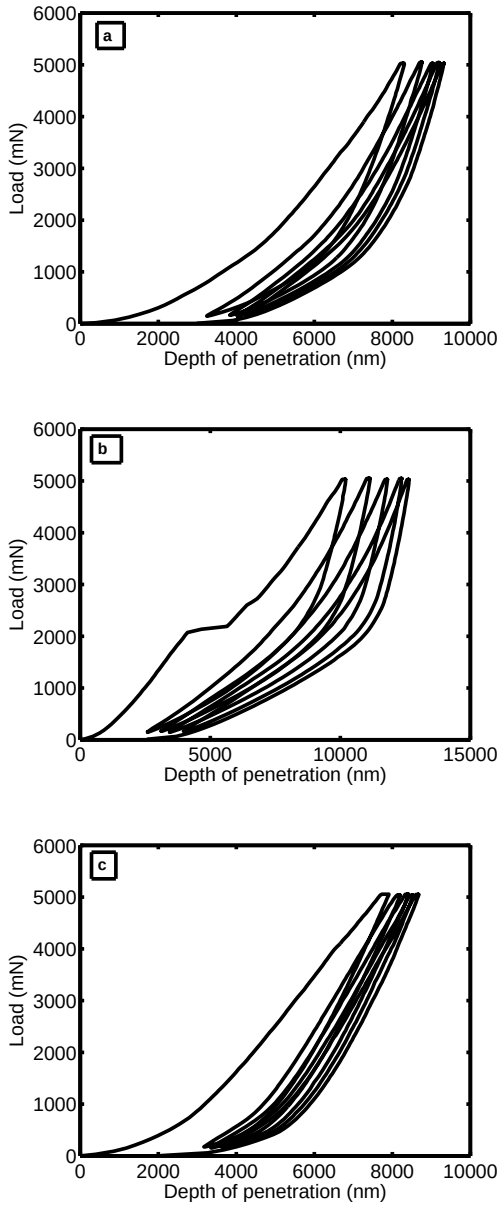

Figure 12: Typical load-displacement curves for the three mixes a) SCC1 b) SCC2 c) SCC3

The typical load displacement plot recorded from microindentation test conducted on the hardened matrix parts of SCC1, SCC2 and SCC3 are shown in Figure 12. Figure 12(b) shows a discontinuity in the load displacement curve of SCC2 which is the phenomenon of microcrack formation generated by the indenter during the first cycle of loading [16]. Using the data of Figure 12 obtained during the indentation tests, the elastic properties are evaluated from the final unloading region of the load versus penetration curve using Oliver and Pharr method [17]. Table 5 shows the elastic modulus (E), the maximum depth of penetration of the indenter (h_{max}) and the hardness (H) of the material computed at the end of each of the five cycles of loading.

Table 5: Typical microindentation results of small specimen of three SCC mixes

Mix	Cycle No.	E GPa	h_{max} nm	Hardness GPa
SCC1	1	81	6218	11.90
SCC2		87	8448	3.700
SCC3		81	6108	13.30
SCC1	2	80	6270	11.30
SCC2		85	9026	3.160
SCC3		72	6691	9.210
SCC1	3	79	6313	11.20
SCC2		84	9303	2.930
SCC3		66	7228	7.260
SCC1	4	78	6332	11.10
SCC2		84	9554	2.700
SCC3		63	7721	6.110
SCC1	5	77	6359	10.80
SCC2		82	9736	2.600
SCC3		61	8139	5.000

It is seen that the elastic modulus and hardness decrease gradually with the number of cycles of loading from first to fifth cycle. This indicates that a gradual degradation of the material is taking place with cyclic indentation. The maximum depth of penetration increases at every cycle of indentation indicating an increase in the plasticity at the tip of the indenter at every cycle. The average response to fatigue loading applied at microlevel indicates that the elastic modulus is almost equal for all the SCC mixes, at initial stage. This implies that the hydration is complete in all the three mixes at 90 days. However, the elastic modulus of the mixes vary during the subsequent cycles. This may be due to the reason that the hardness of the phase which is underlying the indented phase is different from that of the indented phase. In

SCC3, the difference of elastic modulus, hardness and depth of penetration varies widely and this describes that the material beneath the indented phase may have a pore, void or softer phase.

3 CONCLUSIONS

In this study, the behavior of the three different SCC mixes when subjected to variable amplitude fatigue loading and constant amplitude fatigue indentations are studied and discussed. The following conclusions are made:

1. There is a gradual decrease in the stiffness of all the three SCC mixes with increasing number of fatigue load cycles. At failure, the stiffness drops significantly. This behavior indicates that a gradual increase in damage due to microcracking occurs and accumulates, finally leading to a macrocrack formation and subsequent failure.

2. The failure under fatigue loading takes place with a sudden increase in crack length in all the three SCC mixes.

3. The number of fatigue cycles to failure is higher in SCC3 followed by SCC2 and SCC1, although all the concretes were subjected to similar loading pattern. This is due to higher powder content in SCC3 resulting in low porosity and improved microstructure.

4. The size adjusted Paris law used for normal vibrated concrete can predict rate of crack growth in SCC mixes fairly well.

5. The elastic modulus and hardness of the self compacting concrete decreases gradually with increasing number of cycles of indentations indicating a steady degradation of the material.

REFERENCES

[1] L. P. Guo and A. Carpinteri and A. Spagnoli and W. Sun Experimental and numerical investigations on fatigue damage propagation and life prediction of high-performance concrete containing reactive mineral admixtures *International Journal of Fatigue*, 32:227–237, 2010.

[2] M Mahdy,P R S Speare, and A H Abdel-Reheem AFatigue properties of heavy weight, high strength concrete In *Conference Proceedings*,2004.

[3] P. Mondal, S. P. Shah, and L. Marks. A reliable technique to determine the local mechanical properties at the nanoscale for cementitious materials. *Cement and Concrete Research*, 37:1440–1444, 2007.

[4] J. Kim and Y. Kim. Fatigue crack growth of high-strength concrete in wedge-splitting test. *Cement and Concrete Research*, 29:705–712, 1999.

[5] J. K. Kim and Y. Y. Kim. Experimental study of the fatigue behavior of high strength concrete. *Cement and Concrete Research*, 26:1513–1523, 1996.

[6] IS: 12269-1987. *Specification for 53 Grade Ordinary Portland Cement*. Bureau of Indian Standard, .

[7] C 1240 05. *Standard Specification for Silica Fume Used in Cementitious Mixtures*. ASTM International, West Conshohocken, PA, 2009.

[8] C 618 -8a. *Standard Specification for Coal Fly Ash and Raw or Calcined Natural Pozzolan for Use in Concrete*. ASTM International, West Conshohocken, PA, 2009.

[9] Adam M. Neville and Jennifer J. S. Brooks. *Concrete Technology*. Longman Sc and Tech, 1987.

[10] Z.J. Stang and V.C. Li. Experimental study on crack bridging in FRC under uniaxial fatigue tension. *Journal of Materials in Civil Engineering*, 12:66–73, 2001.

[11] Z. P. Bazant and W. F. Schell. Fatigue fracture of high-strength concrete and size effect. *ACI Materials Journal*, 90(5):472–478, 1993.

[12] D. Broek. *Elementary Engineering Fracture Mechanics*. Martinus Nijhoff Publishers, Netherlands, 1982.

[13] P. Paris and F. Erdogan. A critical analysis of crack propagation laws. *Transactions of ASME Journal of Basic Engineering*, 85:528–534, 1963.

[14] Z. P. Bazant and K. Xu. Size effect in fatigue fracture of concrete. *ACI Materials Journal*, 88(4):390–399, 1991.

[15] S. Li, L. Sun, W.Jia, and Z. Wang. The Paris law in metals and ceramics. *Journal of Materials Science Letters*, 14:1493–1495, 1995.

[16] K. Velez, S. Maximilien, D. Damidot, G. Fantozzi, and F. Sorrentino. Determination by nanoindentation of elastic modulus and hardness of pure consituents of portland cement clinker. *Journal of Material Research*, 31:555–561, 2001.

[17] W. C. Oliver and G. M. Pharr. An improved technique for determining hardness and elastic modulus using load and displacement sensing indentation experiments. *Journal of Materials Research*, 7(6):1564–1583, 1992.